An analysis of the production-regeneration system in the coastal upwelling area off N.W. Africa based on oxygen, nitrate and ammonium distributions

by H. J. Minas,[1] T. T. Packard,[2] M. Minas[1] and B. Coste[1]

ABSTRACT

Using the hydrographic and nutrient data from the R/V *Jean Charcot* CINECA-V cruise and Broenkow's (1965) mixing model, we have calculated the biologically induced changes in the oxygen, nitrate and ammonium distribution patterns of the upwelling system off Cape Blanc, N.W. Africa. These changes agree with independent calculations based on ^{14}C-uptake experiments and are consistent with the circulation of the upwelling system. The ratio of nitrogen decrease to oxygen increase in the photic zone is nearly identical to the Redfield ratio of 5.18 μg-at N/ml O_2. In addition to its close couple with nitrate uptake, the oxygen increased directly with the chlorophyll in the offshore-moving waters.

1. Introduction

Nonconservative chemical species in the ocean are partially controlled by the same advective-diffusive processes that control conservative properties, but more importantly, they are controlled by biochemical processes, such as photosynthesis and respiration. Knowing the relative roles of these processes is prerequisite to modeling the flow of nonconservative properties through aquatic ecosystems. This report examines the increase of oxygen in the rising waters of an upwelling ecosystem and the relative roles of photosynthesis and mixing in causing this increase. Broenkow (1965) made a study of this type in the upwelled waters of the Costa Rica Dome in the eastern tropical Pacific. He used oxygen-salinity (O_2-S) and nutrient-salinity (N-S) diagrams to determine that 22% of the oxygen in the surface water was produced by local photosynthesis, 3% was mixed in from the atmosphere and 75% was either mixed in from surrounding waters or was present originally in the upwelled waters. Minas *et al.* (1974) applied a similar analysis to the 1973 Costa Rica Dome upwelling and found that photosynthesis produced only 14% of the oxygen in the surface water, the atmosphere added 7%, and lateral and vertical

1. Station Marine d'Endoume, Laboratoire d'Oceanographie, Faculté des Sciences de Luminy, Case 902, 13288 Marseille, Cedex 9, France.

2. Bigelow Laboratory for Ocean Sciences, McKown Point, West Boothbay Harbor, Maine, 04575, U.S.A.

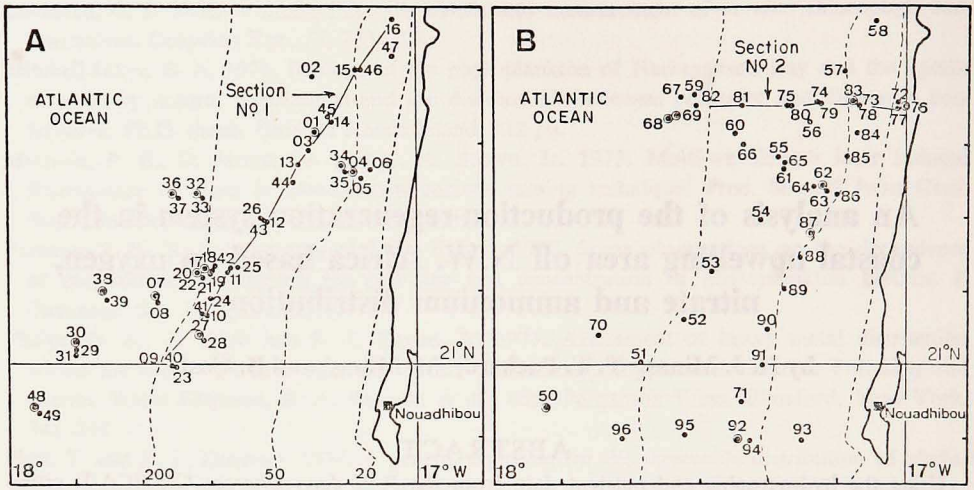

Figure 1. Station locations for the R.V. *Jean Charcot* CINECA-V cruise (Groupe Mediprod, 1976). Panel A: Leg 1 (13-27 March 1974); Panel B: Leg 2 (3-18 April 1974). The lines give the location of the sections in Figures 2 and 3. The circled stations (○) indicate productivity stations; nutrient-hydrography stations are indicated by the points. The bathymetric contours (– – –) are given in meters.

mixing accounted for the remaining 79%. Minas *et al.* (1974) also made a detailed study of the oxygen distribution and its relationship with primary production in the coastal upwelling near Cape Ghir (Morocco) using the O_2-*S* and *N*-*S* diagrams. This paper is an extension of that study as applied to the upwelling off Cape Blanc. However, rather than focusing on the phosphorus part of the *N*-*S* relationships, we have focused on nitrogen and especially the role of ammonium and nitrate.

2. Materials and methods

The data were obtained during the CINECA-*Charcot* V cruise in March-April 1974. The locations are shown in Figure 1. The methods have been described in Groupe Mediprod (1976); the results of an intercalibration study for nutrients and salinity between the R/V J. *Charcot* and *Atlantis* II were published by Frieberts-hauser *et al.* (1975).

Hydrography. Temperature was measured by reversing thermometers (Richter and Wiese) and salinity determinations were performed aboard ship with a Beckman salinometer (Model NO RS 7B). Hydrographic samples for salinity, oxygen and nutrients were taken with NIO bottles, and productivity samples were taken with a 30 L Niskin bottle.

Oxygen. Determinations were made by a modification of the Carpenter (1965) method. The iodine titration was made with a 10 ml automatic burett ("Methrom")

using a 0.015 N sodium thiosulfate solution. This solution was standardized daily by titration with 0.01 N potassium iodate. Oxygen saturation was calculated from the tables of Weiss (1970).

Nutrients. Nitrate was determined immediately after sampling with a Technicon^{R} Auto-Analyzer according to Strickland and Parsons (1968). Ammonium nitrogen was measured by Slawyk and MacIsaac's (1972) modification of the Koroleff (1970) method.

Productivity. Primary production was measured by the classical ^{14}C method of Steemann-Nielsen (1952) with half-day *in situ* incubations at hydrological standard depths. The operating procedures for these determinations are discussed in more detail by Jacques *et al.* (1971) and Minas (1976). Photosynthetic carbon assimilation was determined by the oxygen method (Barnes, 1959; Strickland and Parsons, 1968) using 125 ml Jena glass flasks. The oxygen was measured by the Winkler method (Barnes, 1959) and was converted to carbon according to the equivalence of 1 ml $O_2 = 12/(22.4 \times 1.25) = 0.429$ mg C. A photosynthetic quotient (P.Q.) of 1.25 was assumed.

Chlorophyll. Chlorophyll was determined fluorometrically (Holm-Hansen *et al.*, 1965) according to Neveux (1976).

3. Results

Field Observations. The upwelling off N.W. Africa occurs in several circulation patterns that depend on (1) the shape and width of the continental shelf and slope, (2) the intensity and variability of the local wind field, (3) hydrographic stratification, and (4) latitude (SCOR WE-36, 1975). The following three patterns have been identified from the extensive data suite of the CINECA (Cooperative Investigations of the Northern Part of the Eastern Central Atlantic) program (Mittelstaedt *et al.*, 1975). The first pattern consists of nearshore upwelling with a single upwelling cell on a wide shallow-shelf with water rising to the surface over the shelf in response to weak winds. The second pattern consists of shelf-break upwelling associated with a wide shallow shelf and strong winds. The strongest upwelling in this pattern occurs at the shelf break; weaker upwelling occurs near the coast and sinking occurs at a weak front between the inshore and offshore upwelling cells. The third pattern occurs over deep, narrow shelves and consists of a two celled system with onshore flow occurring above and below the pycnocline. The onshore flow below the pycnocline never reaches the surface, but sinks near the shore and flows offshore along the sea bottom.

During the CINECA *Charcot* V expedition, we worked on the wide shelf, northwest of Cape Blanc (Fig. 1) so we did not observe the third pattern that is characteristic of narrow shelves. We did, however, see a good example of the first pattern

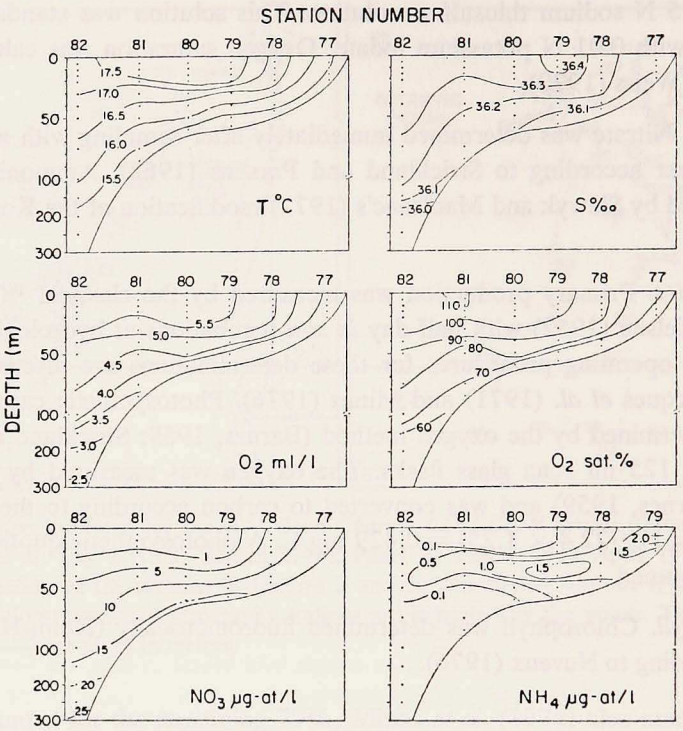

Figure 2. Cross-section No. 2, orthogonal to the coast (ST. 77-82, 14 April, Fig. 1) of hydrography, oxygen and nutrients. Coastal upwelling is indicated between stations 77 and 79. The ammonium maximum extending offshore at about 50 m is assumed in this paper to be the site of nutrient regeneration in a one-celled upwelling condition. There are three proposed origins of this subsurface maximum: (1) from bacterial decomposition of sinking phytoplankton as shown by LeBorgne (1977) for the Cape Timiris upwelling region (~ 20N, 17W); (2) from zooplankton and nekton (Smith and Whitledge, 1977); and (3) from advection from the ammonium-rich nearshore water-column and benthos (Rowe *et al.*, 1977; Codispoti and Friederich, 1978). It is likely that all three mechanisms function from time to time in generating the ammonium maximum.

(single cell) and a fair example of the second pattern (shelf-break upwelling). The single celled pattern was observed during the last part of the cruise (14 April) when the winds were weak and while an orthogonal section was made between inshore station 77 and offshore station 82 (Fig. 1 and Fig. 2). In the upwelled water around station 77, the nitrate was > 10 μg-at/l, the oxygen was $< 80\%$ of its saturation value, and the temperature was $< 16°C$. Offshore, the water warmed up to 17.5°C, the water became saturated with oxygen and the nitrate was depleted (Fig. 2). The most interesting distribution pattern was the tonguelike ammonium pattern (Fig. 2) that extended offshore between 30 and 40 m, a schematic representation of which is shown in Figure 3. The origin of this tongue was the high ammonium (> 1.5

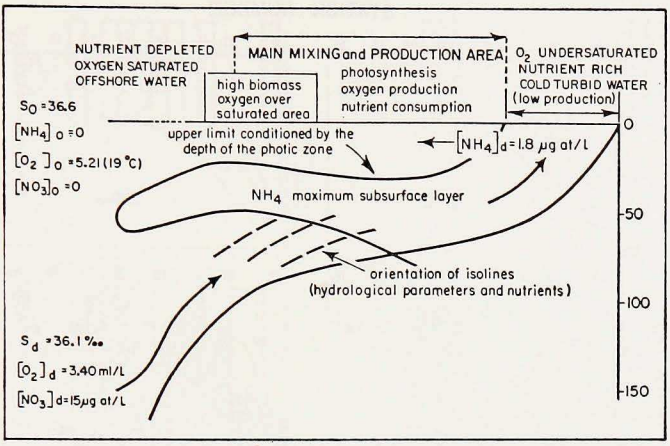

Figure 3. A schematic diagram of a single-celled upwelling and the associated subsurface ammonium maximum in the coastal waters off Cape Corveiro. Along the left side of the figure are given the water characteristics of the seaward-flowing, offshore surface-water and the onshore-flowing, deep (150 m) upwelling source-water. The choice of these values are explained in the text, in Broenkow (1965) and in Minas *et al.* (1974). Their relationships to one another are shown in Figure 6 and they are used to form the mixing lines in Figure 7.

µg-at/*l*) throughout the 25 m water column of station 77 (Fig. 2), but it extended offshore as far as station 81 at mid-depths with values exceeding 0.5 µg-at/*l*.

A shelf-break upwelling pattern was also observed on the cruise. It occurred during a period of strong winds when the ship made the diagonal cross section between the offshore southern station (ST. 9) and the inshore northern station (ST. 16, Fig. 1). That section shows the shelf-break upwelling characteristic of the second pattern (SCOR WE-36, 1975). Rising water at the shelf-break is clearly discernible in the temperature, salinity, nitrate and oxygen panels (Fig. 4). The inshore cell is not as clear; only the bottom water at inshore station 16 suggests upwelling. The subsurface ammonium tongue is completely absent in this section (Fig. 4) suggesting that the circulation and stratification influence the regenerative processes and/or that the organisms effecting the regeneration are aligned differently in the two types of upwelling.

Analysis of all the data from the CINECA-*Charcot* V expedition showed an association (1) between the tonguelike ammonium pattern shown in Figures 2 and 3 and the weak winds that cause nearshore upwelling and (2) between the absence of an ammonium tongue as in Figure 4 and strong winds that cause shelf-break upwelling. These associations are shown in Figure 5. The subsurface NH_4^+ maximum co-occurs most frequently with wind speeds less than 20 knots; at higher wind velocities the subsurface maximum disappears.

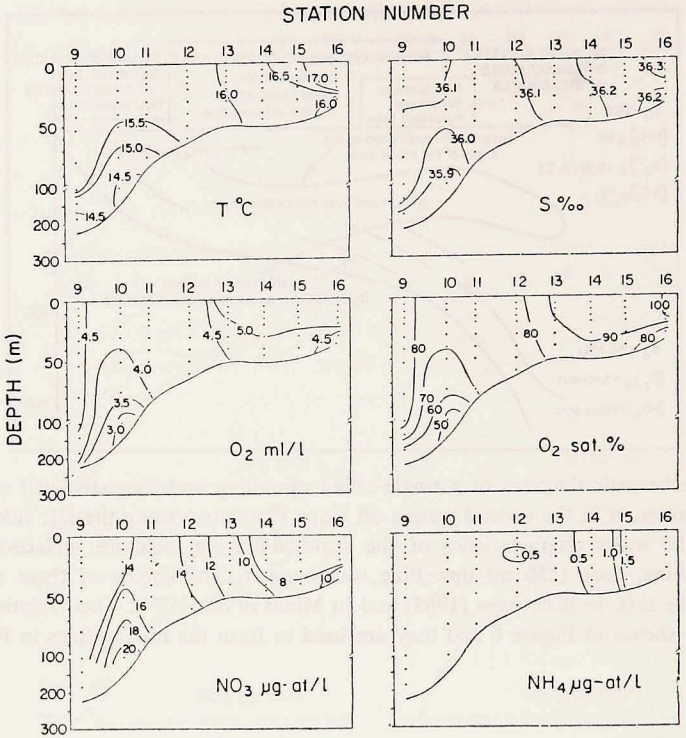

Figure 4. A diagonal cross-section (ST. 9-16, 16 March; Fig. 1) of hydrography, oxygen and nutrients. Shelf-break upwelling is indicated between stations 10 and 12.

Although not as striking as the different ammonium patterns, the different nitrate patterns in the two upwelling situations are nevertheless significant. The nitrate distribution during shelf-break upwelling shows that much more nitrate is injected into the euphotic zone during this type of upwelling than during the one-celled situation. If this nitrate is converted into living matter via photosynthesis it is easy to see that the shelf-break upwelling will stimulate more plankton production than will the one-celled upwelling. Frequently measurements in the immediate vicinity of the upwelling will not reveal this difference because the plankton-rich waters will be more diffused and/or displaced farther offshore in the shelf-break situation as compared to the one-celled situation. However, when integrated over the entire area influenced by upwelled waters, the shelf-break upwelling will be more productive than the one-celled upwelling. An extreme example of how the cumulative productivity is controlled by the nutrient level in the upwelling waters is the Peru Current. Off Peru the nitrate levels in the source water are twice as high as they are off N.W. Africa in the shelf-break upwelling system as we observed it (Fig. 4). The productivity off Peru is correspondingly higher than off N.W. Africa.

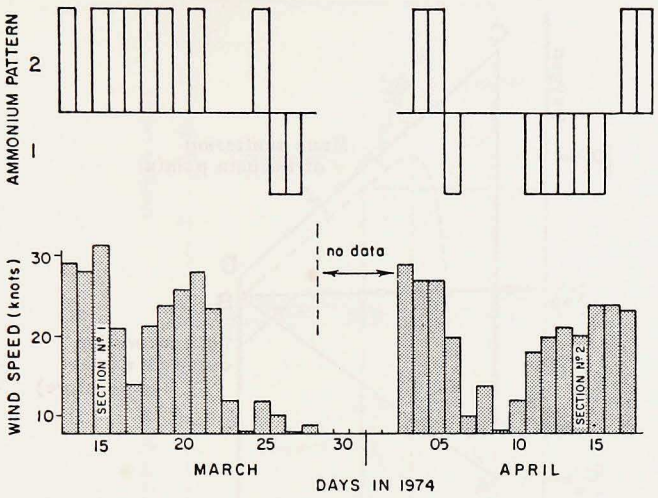

Figure 5. The change from one ammonium distribution pattern to another (No. 1 or 2 in the upper bar-graph) and the co-occurrence of these two patterns with the wind speed (lower bar-graph). Ammonium pattern, No. 1, is characterized by a subsurface maximum (Fig. 2, NH_4^+ panel and Fig. 3) and co-occurs with low winds and nearshore, one-celled upwelling. Ammonium pattern, No. 2 is characterized by a homogenous distribution and co-occurs with strong winds and two-celled upwelling (Fig. 4, NH_4^+ panel).

Oxygen Model. Oxygen and inorganic nutrient salts, such as NO_3^-, NH_4^+, and PO_4^{-3}, are nonconservative properties of seawater, that is to say, their concentrations are controlled, not only by mixing and boundary processes, as are the conservative properties, for example Na^+, Cl^-, and Mg^{+2}, but also by biological activity. Photosynthesis adds O_2 to seawater, but removes nutrient salts and CO_2. Respiration adds CO_2 to seawater, but removes O_2. Remineralization (regeneration) adds nutrient salts to seawater. The conservative and nonconservative fractions of oxygen or nutrient in a seawater sample can be calculated from a mixing line superimposed on an oxygen-salinity or nutrient-salinity plot of a suite of oceanographic data (Fig. 6). The term "nutrient" in this discussion refers to nitrate and ammonium. The mixing line reflects the change in oxygen or nutrient concentration that would occur if neither atmospheric nor biological processes influenced the water chemistry as two water masses were mixing.

For instance, the oxygen content of a water type resulting only from the mixing of two water masses; the first with a salinity, S_A, and an oxygen concentration $\{O_2\}_A$ and the second with a salinity, S_B, and an oxygen concentration $\{O_2\}_B$, can be calculated from the salinity of the sample by the expression: $\{O_2\}_{\text{mix}} = \{O_2\}_A \times (S_{\text{mix}} - S_B)/(S_A - S_B) + \{O_2\}_B \times (S_A - S_{\text{mix}})/(S_A - S_B)$. Examples of the use of this mixing model can be found in Broenkow's (1965) analysis of the Costa Rica Dome

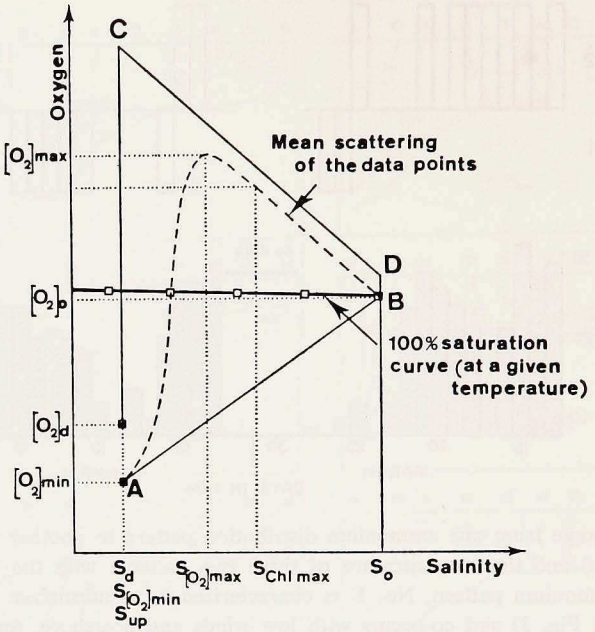

Figure 6. A schematic diagram of the Broenkow (1965) mixing model as developed by Minas *et al.* (1974) to calculate the biological and advective contributions to the oxygen content in coastal upwelling systems. Line A-B is defined by the equation: $\{O_2\}_{mixing} = \{O_2\}_{min}(S_{mix}-S_o)/(S_d-S_o) + \{O_2\}_o(S_d - S_{mix})/(S_d-S_o)$, where $\{O_2\}_{mixing}$ is the predicted oxygen content in a sample with salinity, S_{mix}. This water type occurs when deep water with an oxygen content of $\{O_2\}_{min}$ and a salinity of S_d, are mixed with surface waters having an oxygen content of $\{O_2\}_o$ and a salinity of S_o. The fraction of the deep-water oxygen that is contributed to the new water type is $(S_{max}-S_o)/(S_d-S_o)$; the fraction of surface water oxygen is $(S_d-S_{mix})/(S_d-S_o)$. Line CD represents the maximum amount of oxygen that water of salinity, ranging from S_d to S_o, could produce if its phosphate content was used to support photosynthesis to the extent that 1 μg-at PO_4 would generate 3.09 ml O_2 (Redfield ratio).

and Minas *et al.*'s (1974) analysis of the Moroccan upwelling. The departure of the measured oxygen from its theoretical location on the mixing line reflects the combined effects of photosynthesis ($+\Delta O_2$), respiration ($-\Delta O_2$), and atmospheric exchange. In the case of nitrate, departure from the mixing line reflects phytoplankton nitrate uptake, bacterial denitrification or bacterial nitrification ($-\Delta NO_3$). In the case of ammonium, it reflects phytoplankton ammonium uptake ($-\Delta NH_4$), bacterial nitrification ($-\Delta NH_4$) and/or bacterial and zooplankton ammonium excretion ($+\Delta NH_4$). Throughout this paper we will assume that the signs on the nutrient and oxygen changes are obvious to the reader from the nature of the process involved.

In aerobic phytoplankton-dominated waters, as one finds off N.W. Africa, the oxygen departures from the mixing line reflect net-photosynthesis and atmospheric

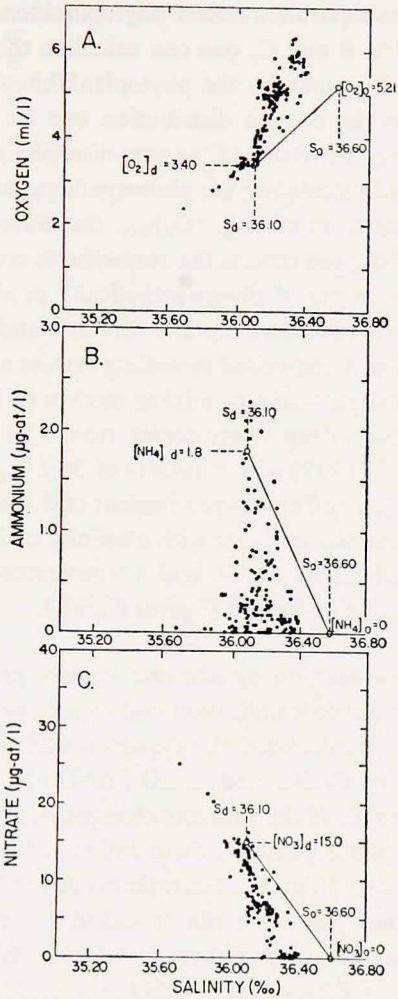

Figure 7. The mixing lines and the observed levels of oxygen, ammonium and nitrate from which the biological oxygen production (ΔO_2), ammonium consumption (ΔNH_4) and nitrate consumption (ΔNO_3) were calculated. The data represent seawater samples drawn from discrete depths at stations 72-92. The mixing lines are defined by points characterizing the deep and surface-water chemical properties (oxygen, nutrients and salinity). Figure 3 shows the location of these waters in a schematic cross-section of the upwelling system. The difference on the ordinate axis between any one data point and its corresponding mixing line represents the amount of oxygen produced (panel A), the associated amount of ammonium extracted from the seawater (panel B), or the nitrate similarly extracted (panel C) by the photosynthetic action of the plankton population. The equations for the mixing lines are: Panel A, $O_2 = 3.62\ S‰ - 127.28$; Panel B, $NH_4^+ = -3.6\ S‰ + 131.76$; Panel C, $NO_3^- = 30.0\ S‰ + 1098$.

exchange and the nutrient-departures reflect phytoplankton uptake. Thus, from the data plotted in Figures 7A, B and C, one can calculate the net photosynthesis and the nitrate and ammonium uptake by the phytoplankton. A check on the effect of atmospheric exchange on the oxygen distribution can be made from the nitrate-salinity plots by invoking the Redfield oxygen-nitrogen atomic ratio of 276:16 (Redfield *et al.*, 1963) and calculating the photosynthetic oxygen production. When this is added to the oxygen from mixing, $\{O_2\}_{mix}$, the difference between the resulting sum and the observed oxygen reflects the atmospheric contribution.

The calculations in this paper of photosynthetically produced oxygen (ΔO_2) and phytoplankton nitrate and ammonium uptake (ΔNO_3^- and ΔNH_4^+) are based on: (1) the conceptual model of a one-celled upwelling system as shown in Figure 3 and (2) oxygen-salinity and nutrient-salinity mixing models of Figures 6 and 7. In our conceptual upwelling model, deep water comes from 150 m, within the poleward undercurrent (Barton *et al.*, 1977) with a salinity of 36.1% (S_d), a nitrate concentration of 15 μg-at/l ($\{NO_3\}_d$), and an oxygen content of 3.4 ml/l ($\{O_2\}_{min}$). It upwells and mixes with offshore surface seawater with a salinity of 36.6% (S_d), no nutrients, an oxygen content of 5.21 ml/l ($\{O_2\}_o$), and a temperature of 19°C. These values serve as the limits for the mixing lines in Figures 6 and 7.

The relationships between nutrient uptake and oxygen production. To investigate the relationships between nutrient utilization and oxygen production in the upwelled waters off Cape Blanc, we calculated the departures of the data from the mixing lines in Figures 7A, B, and C. Denoted as ΔO_2, ΔNH_4 and ΔNO_3, these values are plotted in Figures 8A and B. If the nutrient changes (i.e., ΔNO_3, and ΔNH_4) were closely associated with photosynthesis, their ratios, $\Delta NH_4/\Delta O_2$ and $\Delta NO_3/\Delta O_2$, should be close to 5.18 μg-at N/ml O_2, the ratio predicted by Redfield *et al.* (1963). To test this, regression analyses were run to calculate regression coefficients that are equivalent to the nutrient-oxygen ratios. For $\Delta NH_4/\Delta O_2$, a value of 0.58 μg-at N/ml O_2 was obtained (Fig. 8A); for $\Delta NO_3/\Delta O_2$, the value was 4.51 μg-at N/ml O_2 (Fig. 8B). Thus, ammonium in the water column, although weakly associated with oxygen production ($r = 0.54$), does not change according to the Redfield ratios. Nitrate uptake, on the other hand, is not only closely correlated with oxygen production ($r = 0.91$), but also has a regression coefficient close to the Redfield ratio (i.e., 4.51 μg-at N/ml O_2 versus 5.18 μg-at N/ml O_2).

When both nutrients are added and the resulting total nitrogen change regressed against ΔO_2 as in Figure 8C, the regression coefficient is even closer to the Redfield ratio (i.e., 4.96 versus 5.18). For comparison, the Redfield ratio was drawn in Figure 8C. From this close relationship, one would predict that profiles of the changes in total nitrogenous nutrient (ΔN_{total}) and oxygen in the water column would be parallel. This parallelism is shown in Figure 9, where depth profiles of ΔO_2 and ΔN_{total} have been drawn for each station. The agreement at most stations suggests that

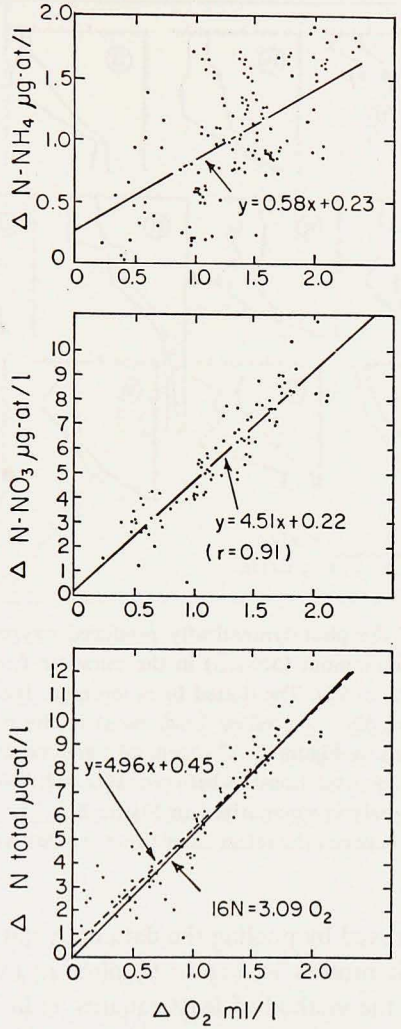

Figure 8. Panel A. The relationship between the biologically produced oxygen (ΔO_2) and the biological ammonium consumption (ΔNH_4) in seawater samples from stations 72 to 92. Vertical profiles of ΔO_2 are shown in Figure 11. The values were calculated from the departure from the ordinate of the individual data points from the respective oxygen-salinity and ammonium-salinity mixing lines in Figure 7. Although the data are scattered ($r = 0.54$), the regression is significant at the 1% level. Panel B. The relationship between the photosynthetically produced oxygen (ΔO_2) in the seawater at stations 72 to 92 and the associated decrease in seawater nitrate (ΔNO_3). Each value is equivalent to the departure of the seawater oxygen or nitrate from the value predicted from the mixing lines in panels A and C of Figure 7. Panel C. The relationship between the photosynthetically produced oxygen (ΔO_2) in the seawater at stations 72 to 92 and the associated summed-decrease in the seawater ammonium and nitrate (ΔN_{total}). As in Figures 8A and 8B, the values of ΔO_2 and ΔN_{total} are based on the variance of the data (along the ordinate axis) from the mixing lines in panels A, B, and C in Figure 7. This regression with $r = 0.89$ is significant at the 1% level.

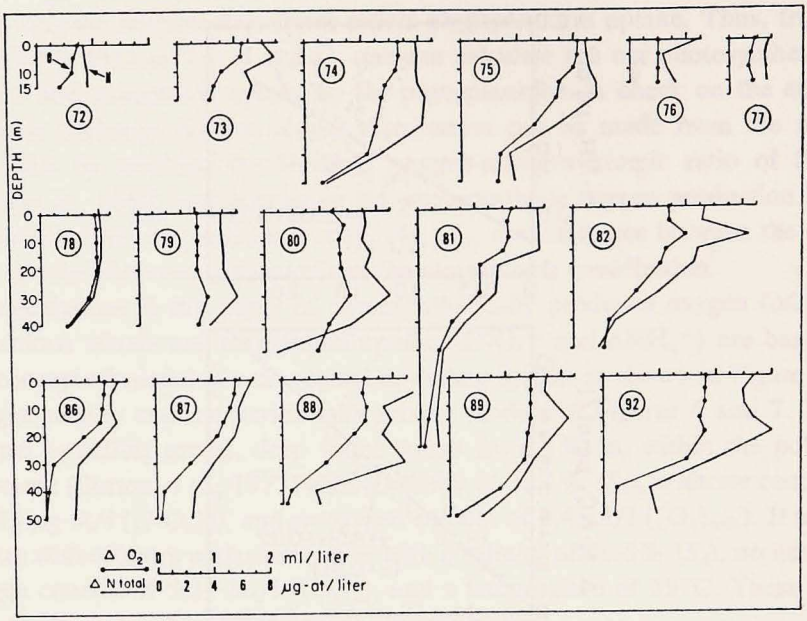

Figure 9. Depth profiles of the photosynthetically produced oxygen (ΔO_2) and the associated decrease of nitrate and ammonium (ΔN_{total}) in the seawater from the upwelling system off Cape Corviero (stations 72 to 92). The dotted lines represent the ΔO_2 depth profiles and the smooth lines represent the ΔN_{total} profiles. Each point in the profiles represents the departure from the mixing lines in Figure 7. The general agreement in the shape of the paired profiles is caused by the good relationship between ΔO_2 and ΔNO_3^- (Fig. 8B) and was predicted by the regression analysis summarized in Figure 8C. The integrated values appear in Table 1. The relationship between the integrals of these profiles is shown in Figure 10.

Figure 8C could be improved by pooling the data on a station basis. This was done by integrating the depth profiles in Figure 9, plotting the integrated values and analyzing the results by the method of least squares as in Figure 10. Table 1 provides a listing of the integrated data. After this smoothing process (Fig. 10), the correlation between nutrient uptake and photosynthesis appears to follow the Redfield ratio even closer than before. Comparing Figures 8C and 10 shows that the correlation coefficient, r, has increased from 0.89 to 0.98 and the regression coefficient increased from 4.96 to 5.23 μg-at N/m/O_2. We conclude from this analysis that changes in the sum of ammonium and nitrate co-vary with photosynthetic oxygen production as Redfield *et al.* (1963) predicted.

4. Discussion

Photosynthesis, the atmosphere and ΔO_2. The general agreement of Figures 8C and 10 with the Redfield N-O ratio suggests that little of the observed oxygen change

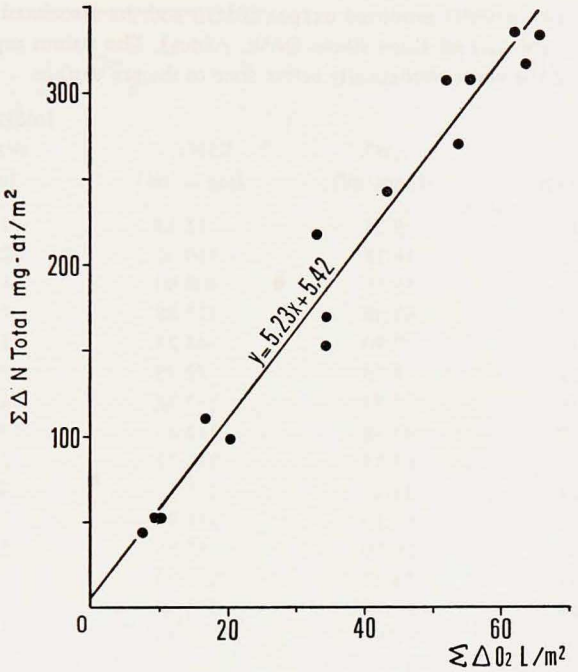

Figure 10. The relationship between the integral amount of oxygen ($\Sigma\Delta O_2$) produced photosynthetically in the water columns of stations 72 to 92 and the associated integral amounts of ammonium and nitrate ($\Sigma\Delta N_{total}$) extracted from the seawater. The correlation coefficient (r) of the regression analysis is 0.98. Each point represents an integrated profile from Figure 9. The basis of the calculation for the data in Figure 9 are explained in the captions of Figures 5-9.

can be associated with atmospheric input during a one-celled upwelling situation. This can be checked by (1) calculating $\{\Delta O_2\}_{biol}$ from daily productivity measurements and the residence time of the seawater on the shelf and comparing the result with the observed ΔO_2; (2) calculating ΔO_2 from 5.18 $\{\Delta N\}$ (the difference between this result and the observed ΔO_2 should be the atmospheric contribution to ΔO_2); (3) calculating the atmospheric contribution directly from Redfield's (1948) equation for oxygen exchange at the sea surface. From the daily productivity measurements, examples of which are shown in Figure 11, one can calculate the daily oxygen production (+ ΔO_2). At stations 76, 83 and 92, the phytoplankton produced 1.7, 7.6 and 17.6 l O_2 day^{-1} m^{-2}. For stations 76 and 92, the ΔO_2 given by the model are: 7.5 and 51.9 l O_2/m^2. The length of time required to achieve these levels of ΔO_2 by the phytoplankton would be 4.4 and 2.9 days, respectively, for stations 76 and 92. Since station 76 is in the upwelling source water, some of its ΔO_2 must come from mixing because its seawater could not have been in the euphotic zone for the

Table 1. The photosynthetically produced oxygen ($\Sigma\Delta O_2$) and the associated decrease in nitrate and ammonium ($\Sigma\Delta N_{total}$) off Cape Blanc (N.W. Africa). The values represent integrations from the bottom of the photosynthetically active zone to the sea surface.

Station	$\Sigma\Delta O_2$ (liters/m^2)	$\Sigma\Delta N_{total}$ (mg-at/m^2)	Integration depth (m)
72	9.23	52.15	15
73	16.78	110.63	20
74	55.55	308.60	40
75	63.48	317.88	40
76	7.50	44.25	15
77	9.35	52.45	20
78	34.30	152.78	40
79	43.18	242.48	40
80	65.38	335.28	50
81	33.15	218.38	30
82	62.10	336.88	50
86	20.20	97.60	20
87	34.35	169.95	30
89	53.73	271.10	40
92	51.88	308.13	30

required 4.4 days. However, since station 92 is about mid-shelf (Fig. 1), the offshore-flowing upwelled-seawater would have resided long enough in the euphotic zone for the phytoplankton to have generated the observed ΔO_2. To check this, one can calculate a residence time from the current data of Mittelstaedt *et al.* (1975) and the upwelling velocity of Barton *et al.* (1977). The upwelling velocity is about 3.6 m/hour. Thus, for the 15 m euphotic zone, the plankton in the seawater would only have had 4.1 hours in which to photosynthesize. However, the water flows offshore at 4.3 km/day, at which rate it will take nearly seven days to reach mid-shelf; ample time to generate the observed ΔO_2 by photosynthesis.

Another way of investigating the source of the oxygen is to calculate the O_2 influx from the oxygen saturation data (Figs. 2 and 4) and from the oxygen exchange coefficient (piston velocity). The exchange coefficient has been studied in the laboratory and at sea by many investigators; see Kester (1975) for a review. The coefficients from field and laboratory studies agree in general, but vary greatly with wind velocity. Downing and Truesdale (1955) and Kanwisher (1963) showed that the exchange coefficient is a function of the square of the wind velocity. During our study of the N.W. African upwelling, the wind velocity in the three days preceding the occupation of section 2, averaged 20 knots. According to Kester's (1975) review, the exchange coefficient under these conditions would be $8.4 \cdot 10^3$ *l* O_2 m^{-1} atm^{-1} month^{-1}, if we use the units of Redfield (1948). At station 77, where the surface seawater was only 70% saturated, we can calculate the rate of oxygen influx from

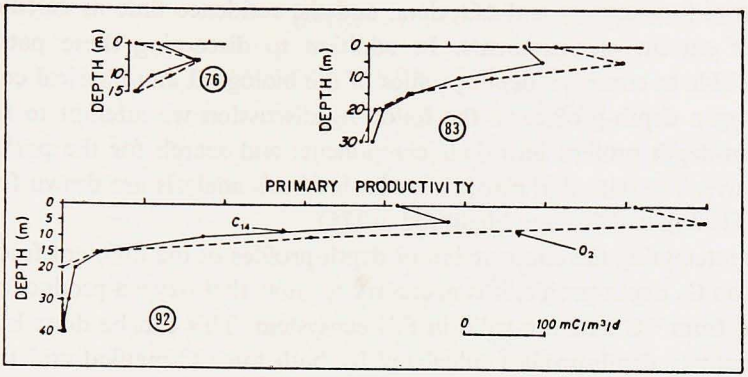

Figure 11. Comparison between photosynthetic productivity measured by the ^{14}C method and by the oxygen method (Strickland and Parsons, 1968). Incubations were made *in situ* at stations 76, 83, and 92. The integrated productivities (g C d^{-1} m^{-2}) for the three stations were 0.66, 2.54, and 4.74 as measured by the ^{14}C method; and 0.73, 3.26, and 7.53 as calculated from the oxygen method.

the expression: $\{\Delta O_2\}_{atm} = E\ (P-p)$, where E is the oxygen exchange coefficient, $8.4 \cdot 10^3$ *l* O_2 m^{-1} atm^{-1} $month^{-1}$, P is the partial pressure of oxygen in the atmosphere (0.21 atm) and p is the partial pressure of oxygen in the surface seawater (0.15 atm). Thus, for station 77, the rate of influx equals 16 *l* O_2 m^{-2} day^{-1}. For station 78, where the seawater was 90% saturated, the rate of influx was 5.7 *l* O_2 m^{-2} day^{-1}. Farther offshore, the seawater was saturated with O_2; so the rate of O_2 influx had to be zero.

The productivity at station 76 was 1.7 *l* m^{-2} day^{-1}, so at this location, atmospheric input would have dominated the oxygen changes at the sea surface. Offshore, the productivity becomes much greater and the atmospheric input becomes zero. Since most of the stations were taken in the offshore waters where oxygen saturation is near 100% (Figs. 1 and 2), it becomes understandable why the observed ΔO_2 are largely explained by the Redfield ratio (Figs. 8C and 10). In fact, if we calculate $\{\Delta O_2\}_{biol}$ from the Redfield N:O ratio and ΔN_{total}, we find that there is no consistent pattern in the small differences between $\{\Delta O_2\}_{biol}$ and the observed ΔO_2. We conclude from this analysis that the origin of the oxygen in the one-celled upwelling system, beside the amount introduced by the rising waters, stems from photosynthesis and not from the atmosphere.

Phytoplankton productivity. Analysis of the ΔO_2 data (Table 1) and its relationship with productivity data should reveal certain patterns. Among these one would expect: (1) an increase in ΔO_2 with increasing residence time of upwelled water in the euphotic zone; (2) an increase in phytoplankton biomass in waters characterized by increasing ΔO_2; and (3) a close correspondence between the residence time as cal-

culated from productivity and ΔO_2 data, and the residence time as calculated from cross-shelf current measurements. In addition to discerning these patterns, one should be able to construct depth profiles of the biological and physical components of the oxygen depth-profile. In the following discussion we attempt to fractionate the oxygen-depth profiles into their components and search for the patterns mentioned above. The data that provide the basis of this analysis are drawn from Table 1, Minas (1976), and Groupe Mediprod (1976).

Before attempting the construction of depth-profiles of the different fractions that comprise an O_2 depth-profile, it is necessary to show that oxygen production profiles calculated from ^{14}C data are valid in this ecosystem. This can be done by comparing productivity depth-profiles calculated by both the ^{14}C method and the oxygen method. Such a comparison for three stations is shown in Figure 11. In the NH_4^+-rich waters of station 76, the ^{14}C-derived profile and O_2-derived profile agree; but in the NH_4^+-deficient, NO_3^--rich waters of stations 83 and 92, the O_2-based profile shows greater productivity near the sea surface. The recent work of Williams *et al.* (1979) explains this discrepancy. To calculate productivity in carbon units from productivity measurements based on oxygen determinations, one normally uses a value of 1.25 for the photosynthetic quotient (P.Q.). The O_2-based profiles in Figure 11 were calculated this way. However, Williams *et al.* (1979) have shown that the P.Q. can vary from 1.25 for NH_4^+-based phytoplankton growth to 1.7 for NO_3^--based phytoplankton growth. If the profiles for the NO_3^--rich, NH_4^+-poor stations 83 and 92 were calculated with a P.Q. of 1.7, the O_2-based profile would be closer to the ^{14}C-based profiles. In spite of these small differences, the general agreement between the ^{14}C and oxygen based productivity profiles permits us to use the ^{14}C productivity to calculate the daily biological oxygen production. So, from this type of productivity data (Minas, 1976), from the chemistry data (Groupe Mediprod, 1976) and from the model (Figs. 6 and 7), we constructed depth profiles of the different oxygen fractions that comprise the observed O_2 profile. Figure 12 presents two such oxygen depth profiles partitioned into four fractions: the original oxygen in the upwelled seawater; the oxygen mixed in from overlying and adjacent waters (from the mixing line in Fig. 7); the oxygen produced biologically, since the seawater was upwelled (from the model (Figs. 6 and 7)); and the oxygen produced biologically during the day the station was made (Minas, 1976). The atmospheric input of oxygen, as previously discussed, and the zooplankton oxygen consumption (Packard, 1979) were considered negligible. The profiles show (1) both the oxygen from mixing and the oxygen from photosynthesis, increasing toward the surface; (2) the relatively small amount of the oxygen from mixing; and (3) that the daily productivity comprises a relatively large fraction of the total biologically-derived oxygen.

As mentioned previously, there should be a close correspondence between the residence time as calculated from productivity and ΔO_2 data and the residence time

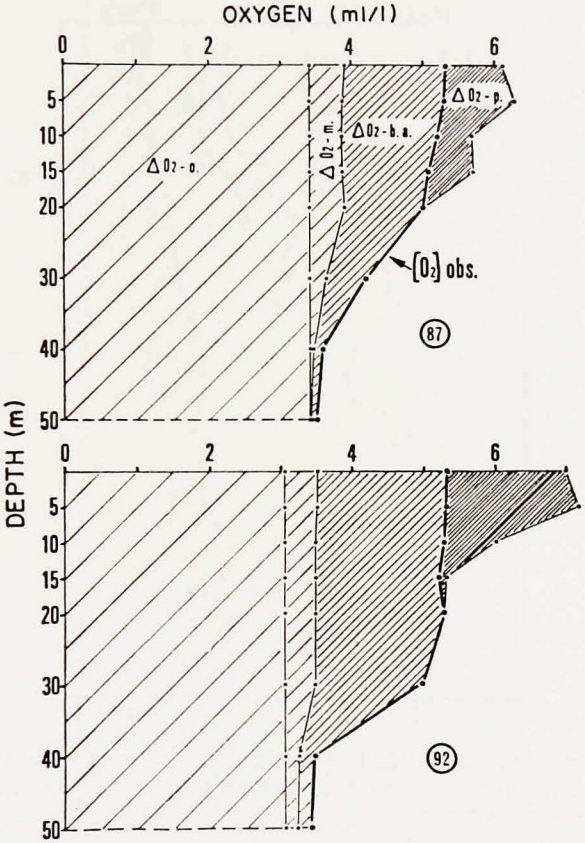

Figure 12. The depth distribution of the net daily oxygen production ($\Delta O_2 - P$), the accumulated net oxygen of biological and atmospheric origin ($\Delta O_2 - ba$), the oxygen mixed in from other waters (ΔO_2 — m), and the original oxygen in the upwelled water (ΔO_2 — 0) at stations 87 and 92.

as calculated from the cross-shelf current measurements. In addition, the ΔO_2 should increase seaward across the upwelling system. First we will calculate the residence time from the productivity and ΔO_2 data. At station 76 and 92, the daily productivity (Minas, 1976; (P.Q. = 1.7)) represents 23% and 34% of the total biologically-derived oxygen (Table 1). The time to generate the ΔO_2 can be calculated by inverting the percentages and multiplying by 100. For stations 76 and 92, 4.4 and 3 days are required. This "build-up" time is consistent with the residence time of the upwelled shelf waters calculated from current velocities in the "surface-drift" layer. Barton *et al.* (1977) find a current velocity of 5 cm/sec for this layer and an upwelling velocity of 0.1 cm/sec. For the inner 10 km of the shelf where the depth is about 50 m, the residence time is 2.9 days. This calculation assumes that the sea-

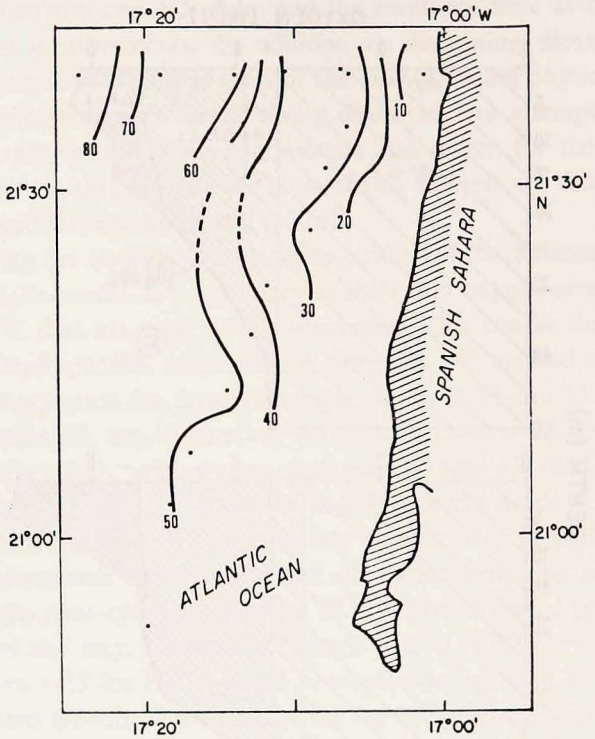

Figure 13. The offshore increase in the biologically generated oxygen (ΔO_2) in the Cape Blanc upwelling system. These values were calculated from the model as shown in Figures 6 and 7, and are expressed as liters O_2/m^2.

water near the coast upwells through 50 m water column and moves 10 km offshore (i.e., the one-celled circulation model). One would thus expect to find an offshore gradient in ΔO_2 as photosynthetically produced O_2 accumulates in the seawater. Figure 13 shows a contour plot of the ΔO_2 data from Table 1. As predicted, low values of ΔO_2 (<40 l/m^2) are found near the coast and higher ones (ΔO_2 >50 l/m^2) are found offshore.

This ΔO_2 distribution pattern observed here is similar to the offshore increase in pH that Simpson and Zirino (1980) have reported for the Peruvian upwelling system. In both cases, the increase in pH and the increase in ΔO_2 serve as indices of the net production of the planktonic community. In fact, in areas where exchange across the sea surface is minimal (i.e., when the % saturation of $O_2 \approx 100\%$ as in Figs. 2 and 3), ΔO_2 becomes a better index of community net production than particulate carbon. This is because some of the organic carbon produced by the phytoplankton is lost by sinking, grazing and export from the area. The oxygen, however, remains in the water as a record of the photosynthesis from an earlier time.

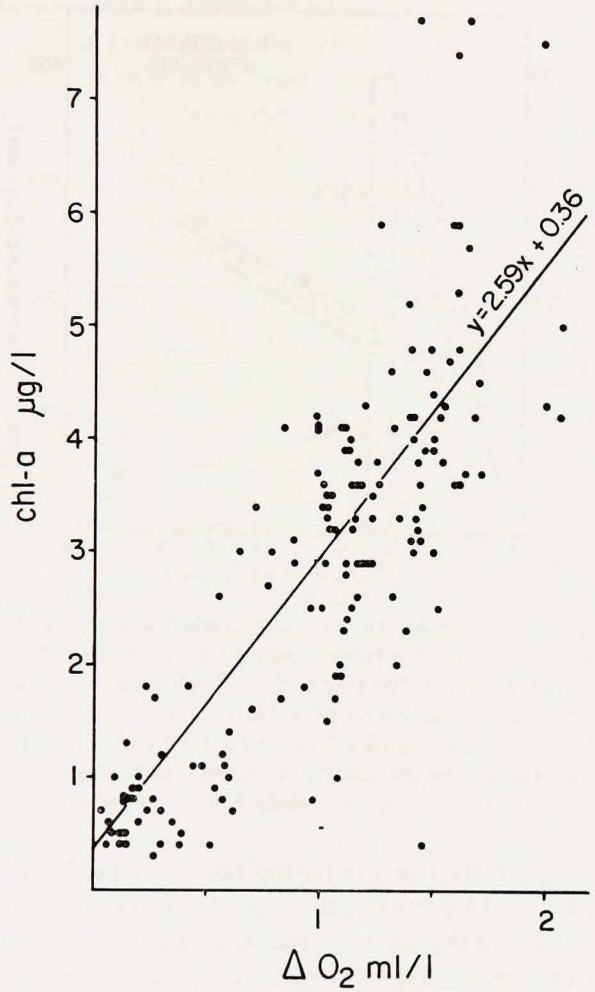

Figure 14. The relationship between chlorophyll *a* and biologically produced oxygen (ΔO_2) in the Cape Blanc upwelling system. The correlation coefficient (*r*) was 0.73.

In spite of the losses from the phytoplankton, one would expect phytoplankton biomass to accumulate with distance away from the upwelling source and accordingly chlorophyll and ΔO_2 should show some correlation. Figure 14 shows that such a correlation is characteristic of the Cape Blanc upwelling system; the regression equation for this relationship was chl $a = 2.6\ \Delta O_2 + 0.4$. If we convert the ΔO_2 from this regression equation to the carbon equivalent by invoking the Redfield *et al.* (1963) oxygen-carbon ratio, we generate a relationship between biologically produced carbon and observed chlorophyll that is plotted in Figure 15. Note that this

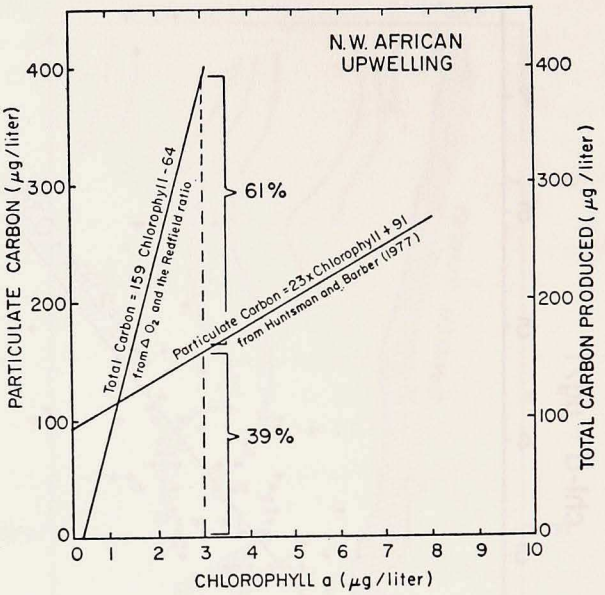

Figure 15. The predicted relationship between photosynthetically produced carbon and chlorophyll, and the observed relationship between particulate carbon and chlorophyll as measured by Huntsman and Barber (1977). The predicted relationship was calculated from the Redfield *et al.* (1963) oxygen-carbon relationship (276/106 by atoms) and the Chl $-$ ΔO_2 regression equation from Figure 14. The disparity between the total carbon and the PC for a chlorophyll value of 3 $\mu g/l$ represents the amount of carbon that has been lost to the benthos, the deep water column, the dissolved fraction, and the biomass of higher trophic levels.

carbon represents the carbon in the phytoplankton as predicted from the model (Figs. 6 and 7). Figure 15 compares the predicted carbon-chlorophyll relationship with the observed relationship as measured by Huntsman and Barber (1977). The discrepancy between the two lines represents the amount of newly produced carbon lost to the deep water column and benthos, to excretion, and to grazing and the production of biomass in the higher trophic levels. For a value of 3 $\mu g/l$ chlorophyll, which was average during our cruise (Fig. 12), more than 60% of the newly produced carbon has left the phytoplankton carbon pool. In a slightly different manner Ryther *et al.* (1971) observed similar results for the Peruvian upwelling system; although there, they concluded that most of the newly produced carbon had been converted to anchovy biomass and that relatively little had been lost to sinking. Off N.W. Africa, the relative importance of the different losses has not been assessed.

Ammonium distribution. The analysis of ammonium distribution is particularly interesting, since ammonium constitutes the principal nitrogen source for the so-called regenerated production. Comparing the different panels in Figure 8 leads one to conclude that the relationship between total nitrogen uptake ($\Sigma\ \Delta NO_3 + \Delta NH_4$) and

the oxygen production (ΔO_2) is dominated by nitrate uptake rather than ammonium uptake. Another way of investigating the relative roles of nitrate and ammonium uptake is to calculate a version of the relative preference index (RPI) as defined by McCarthy *et al.* (1977). The index is calculated for each nutrient and is equivalent to the relative rate at which the nutrient is taken up by the phytoplankton normalized by the relative abundance of that nutrient in seawater. It was originally based on volume-specific uptake rates, ρ. The RPI_{NH_4}, for example is:

$$\frac{\rho NH_4}{\rho_{NH_4} + \rho_{NO_3} + \rho_{NO_2} + \rho_{urea}} \Big/ \frac{\{NO_4\}}{\{NH_4^+\} + \{NO_3\} + \{NO_2\} + \{urea\}}$$

Our data suite does not yield such short term rates; it yields the cumulative effect of these rates on the nutrient supply. Furthermore, we do not have NO_2^- and urea data to consider, thus our RPI calculations will represent the overall relative uptake of ammonium and nitrate over the entire one-celled upwelling system rather than the short term physiological uptake rates that the RPI was originally designed for. A problem with this type of data analysis arises with the ammonium uptake. If regeneration occurs at the same site in the water column and is mediated by microorganisms, then both ΔNH_4 and ρNH_4 will underestimate the true ammonium uptake whether it be cumulative over the whole system or whether it be short term as during a $^{15}NH_4^+$ uptake experiment. This error will not be too significant if: (1) regeneration occurs mainly below the euphotic zone (i.e., at 50 m as in Fig. 2) and (2) the calculation of ΔNH_4 is based on the high salinity water at the inshore root of the ammonium maximum as shown in Figures 2 and 7. Proceeding on these assumptions, we calculated RPI_{NO_3} and RPI_{NH_4} and obtained values that ranged so near to one that we concluded that uptake was proportional to the ratio of these nutrients in the source water at the bottom of the nearshore region of the upwelling system (Fig. 2).

In an attempt to test the preceding conclusion as well as our general understanding of the mechanisms that control the ammonium distribution in the upwelling system, we propose a simple ammonium model:

$$\{NH_4^+\} = \{NH_4^+\}_{mix} - p\,\Delta NO_3^- \qquad (1)$$

where $\{NH_4^+\}$ is the predicted ammonium concentration at any point in the upwelling system; $\{NH_4^+\}_{mix}$ is the ammonium concentration that is predicted from the mixing line (Fig. 7B); ΔNO_3 is the biological nitrate uptake rate (i.e., the difference between the observed NO_3^- and the NO_3^- predicted from the mixing line (Fig. 7C)); and p is the ratio of NH_4^+ uptake to NO_3^- uptake. If, as we have just concluded, this ratio is the NH_4-NO_3 ratio in the source water then $p = 1.8/15 = 0.12$. We used this value for p in equation (1) to calculate the ammonium distribution. Figure 16 shows the outcome. The computed NH_4^+ along section 2, (Fig. 1) is in close agreement in the surface waters of the central part of the upwelling system.

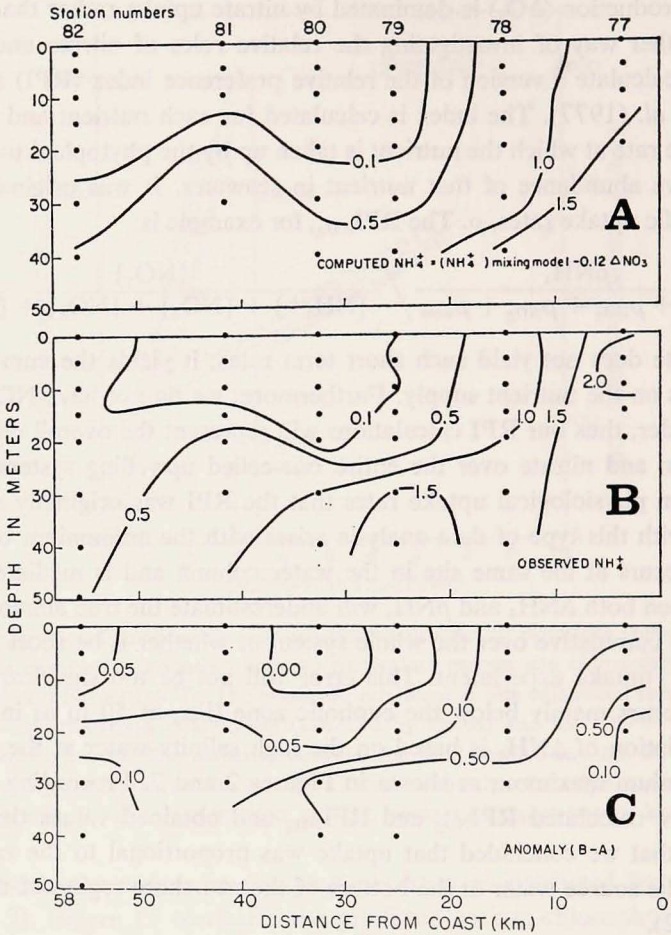

Figure 16. The ammonium distribution computed (Panel A) for section 2 (Fig. 1) off Cape Blanc from the equation: $\{NH_4^+\} = \{NH_4^+\}_{mix} - 0.12\ \Delta NO_3^-$ (see text). The calculated distribution is compared to the observed ammonium distribution (Panel B). The difference between the computed and observed distribution is shown in Panel C. The units are: μg-at NH_4^+/l.

A marked anomaly in the predicted NH_4^+ distribution occurs at station 77 in the near coastal waters (Fig. 16). It may be explained by the uncertainty that is associated with the choice of the mixing-line end points. Nevertheless, the relatively good agreement between the predicted and observed ammonium distribution leads us to conclude that: (1) the principal source of ammonium in the region is the subsurface water over the continental shelf rather than in the euphotic zone; (2) the high productivity in the upwelling system is based on the utilization of nitrate; and (3) that the uptake ratios of the two nutrients are in proportion to their abundance

in the source water. This latter conclusion agrees with Figure 3 in Eppley (1979) which demonstrates that the ratio of new production to total production increases in highly productive waters. On our cruise new production was 90% of the total.

Effects of mixing in strong shelf break upwelling as exhibited in an oxygen-salinity diagram (Fig. 17). So far we have examined the oxygen-nutrient relations during the one-celled upwelling situation (Fig. 3). If we examine the data from the shelf-break upwelling situation in the same way, we find that the oxygen in the low-salinity source water is higher than it was in the one-celled upwelling situation. Figure 17 shows the difference between the two data suites. Envelope A encloses the data used in the model (stations 72 to 96); envelope B encloses all the data from the cruise.

The principal difference between the two envelopes is a high frequency of points showing an increased oxygen concentration (4.5 ml) for lower salinities near 36‰, which is the salinity of the source water in the shelf-break upwelling. The strong wind conditions agitating the sea surface and mixing waters to great depths is the likely cause of the greater aeration. This is the same reason why the biological contribution to the ΔO_2 in these waters is low (Huntsman and Barber, 1977). When these waters have generated all the potential oxygen predicted from the Redfield ratio, their O_2-*S*‰ type will fall above the C-D line regardless of their dilution (Figs. 6 and 17). Even before the waters reach this condition they will start to de-gas, giving off oxygen to the atmosphere. The net amount given off will be equivalent to the level of preformed nitrate in the source water and to the difference in oxygen solubility dictated by the temperature decrease as the seawater passes through the upwelling system from source to offshore. This net flux is the result of: (1) an invasion of oxygen during intense mixing before photosynthesis influenced the oxygen levels; (2) de-gassing of oxygen after the phytoplankton had generated it according to the Redfield ratio. The net flux will always be equal to the level of preformed nutrients in the source water as modified by the solubility differences between the source and offshore water. For example, in the one-celled upwelling (Fig. 17), where the source water contains 3.4 ml O_2/l and 15 μg-at NO_3^-/l, the AOU is 2.25 ml O_2/l and the preformed nitrate is 3.35 μg-at/*l*. According to Redfield *et al.* (1963), this level of preformed NO_3^- is equivalent to 0.65 ml O_2/l at the temperature of the source water (15.5°). At the offshore warmer surface waters even more oxygen will be lost which can be calculated from the solubility tables of Weiss (1970).

5. Summary and conclusions

1. Analyses of the CINECA-*Charcot*-V data from the N.W. African upwelling system off Cape Corveiro show first an association and co-occurrence between weak winds, a simple one-celled circulation system and a midwater tonguelike subsur-

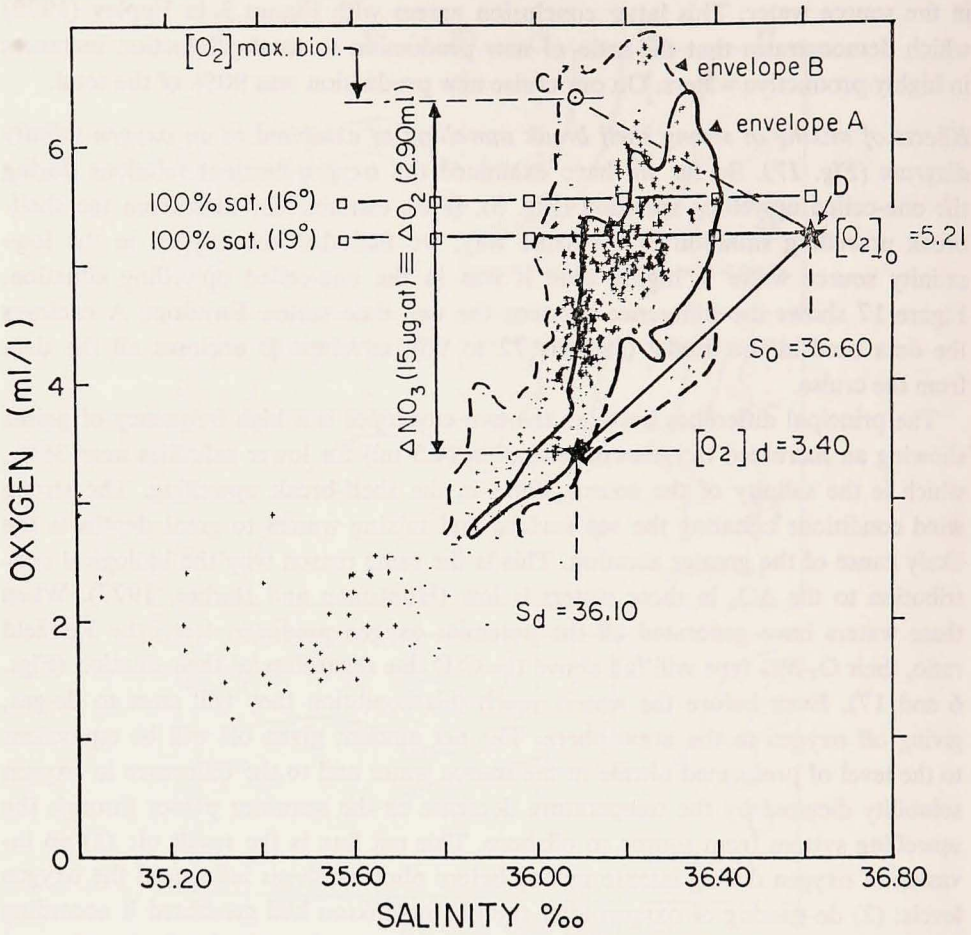

Figure 17. Oxygen-salinity diagram for the data from the CINECA-*Charcot* V cruise. Envelope A encloses the data from stations 72 to 92 which are the data used in the model (Figs. 6-10). Envelope B encompasses all the data from the cruise. The line between the two starred points represents the mixing line in Figures 6 and 7A. The difference between this mixing line and line CD represents the oxygen produced biologically if all the nitrate is consumed in the water by photosynthesis according to the Redfield model (Redfield *et al.*, 1963). All the points above the 100% saturation lines represent super-saturated samples. At point C, with a temperature of 19°C, the seawater would be 121% saturated with oxygen.

face ammonium maximum extending seaward over the N.W. African shelf; and second, an association between strong winds, a shelf-break upwelling system (two-cell upwelling) and a uniform ammonium distribution over the shelf.

2. Oxygen production and nutrient uptake were calculated by analysis of the salinity-oxygen and salinity-nutrient diagrams, which were constructed from the data during the one-celled upwelling situation.

3. From this analysis, we concluded that the increase in oxygen in the photic zone stems largely from photosynthesis and that it co-varies with changes in the sum of nitrate and ammonium according to the O/N ratio of Redfield *et al.* (1963). We also concluded that the atmospheric input of oxygen is relatively small and confined to the undersaturated waters close to the coast.
4. Autotrophically produced carbon (ΔC) was calculated from the photosynthetically produced oxygen (ΔO_2). From this ΔC we subtracted the standing level of phytoplankton carbon pool as calculated from Huntsman and Barber (1977). The difference which equaled about 60% of the carbon produced (ΔC), represents the carbon exported to higher trophic levels, the carbon transformed into dissolved organic carbon and/or the carbon that sinks to the bottom.
5. The productivity (net) is based largely on nitrate-uptake (new production) rather than on ammonium-uptake (regenerated production). Our analysis indicates that the ratio, new production/regenerated production was 90% during this expedition.
6. The oxygen distribution in the two upwelling situations (i.e., the shelf-break and the one-celled system) shows that the aeration is much greater during shelf-break upwelling. In both types of upwelling the net flux of oxygen across the air-sea interface is positive to the atmosphere and is equivalent to the amount of preformed nitrate in the source water.
7. Shelf-break upwelling is potentially more important in stimulating plankton production than is one-celled upwelling. However, the areal extent of its influence is much greater and this can mask its importance if only the freshly upwelled water is sampled.

Acknowledgments. This study was supported from France by CNRS contracts RCP-247, GRECO 130034, and LA-41; and from the USA by ONR contract N00014-76-C-0271, and NSF Grants OCE-80-11187 and C-OTH-0086. We thank M. C. Bonin and P. David for their assistance with the computations and with the chemical analyses; and Y. Collos, G. Slawyk, L. Codispoti and C. Garside for stimulating discussions.

REFERENCES

Barber, R. T. and S. A. Huntsman. 1975. JOINT I carbon, chlorophyll and light extinction—R/V *Atlantis* II cruise 82. CUEA Data Report 14, 165 pp.

Barnes, H. 1959. Apparatus and Methods of Oceanography. Part One: Chemical. G. Allen and Unwin, Ltd., London, 341 pp.

Barton, E. D., A. Huyer and R. L. Smith. 1977. Temporal variation observed in the hydrographic regime near Cabo Corveiro in the northwest African upwelling region, February-April 1974. Deep-Sea Res., *24,* 7–23.

Broenkow, W. W. 1965. The distribution of nutrients in the Costa Rica Dome in the eastern tropical Pacific Ocean. Limnol. Oceanogr., *10,* 40–52.

Carpenter, J. H. 1965. The accuracy of the Winkler method for dissolved oxygen. Limnol. Oceanogr., *10,* 135–140.

Codispoti, L. A. and G. E. Friederich. 1978. Local and mesoscale influences on nutrient variability in the Northwest African region near Cabo Corveiro. Deep-Sea Res., *25,* 751–770.

Downing, A. L. and G. A. Truesdale. 1955. Some factors affecting the rate of solution of O_2 in water. J. Appl. Chem., *5,* 570 pp.

Dugdale, R. C. and J. J. Goering. 1967. Uptake of new and regenerated forms of nitrogen in primary productivity. Limnol. Oceanogr., *12,* 196–206.

Eppley, R. W., E. H. Renger and W. G. Harrison. 1979. Nitrate phytoplankton production in southern California coastal waters. Limnol. Oceanogr., *24,* 483–494.

Friebertshauser, M. A., L. A. Codispoti, D. D. Bishop, G. E. Friederich and A. A. Westhagen. 1975. JOINT I hydrographic station data. R/V *Atlantis* II cruise 82. CUEA Data Report, 18, 243 pp.

Groupe Mediprod. 1976. Résultats de la campagne CINECA-5-J.CHARCOT-CAPRICORNE 7403 (1er Mars au 20 Avril 1974). Publ. CNEXO, sér. Résultats de campagnes à la mer, 10.

Holm-Hansen, O., C. I. Lorenzen, R. W. Holmes and J. D. H. Strickland. 1965. Fluorometric determination of chlorophyll. J. Cons. Perm. Intern. Explor. Mer., *30,* 3–15.

Huntsman, S. A. and R. T. Barber. 1977. Primary production off northwest Africa: the relationship to wind and nutrient conditions. Deep-Sea Res., *24,* 25–33.

Jacques, G., H. J. Minas, M. Minas and P. Nival. 1971. Influence des conditions hivernales sur les productions phyto-et zooplanctoniques en Méditerranée nord-occidentale. II. Biomasse et production phytoplanctonique. Mar. Biol., *23,* 251–265.

Kanwisher, J. 1963. On the exchange of gases between the atmosphere and the sea. Deep-Sea Res., *10,* 195–207.

Kester, D. R. 1975. Dissolved gases other than CO_2, *in* Chemical Oceanography, *8,* 498–556. J. P. Riley and G. Skirrow, eds., Academic Press, Inc., New York, 606 pp.

Koroleff, F. 1970. Information on techniques and methods for seawater analysis. International Council for the Exploration of the Sea, Interlaboratory Report, *3,* 19–22.

LeBorgne, R. P. 1978. Ammonia formation in Cape Timiris (Mauritania) upwelling. J. Exp. Mar. Biol. Ecol., *31,* 253–265.

McCarthy, J. J., W. R. Taylor and J. L. Taft. 1977. Nitrogenous nutrition of the plankton in Chesapeake Bay. I. Nutrient availability and phytoplankton preferences. Limnol. Oceanogr., *22,* 996–1011.

Minas, H. J., L. A. Romana, T. T. Packard and M. C. Bonin. 1974. La distribution de l'oxygène dans un upwelling côtier (NW de l'Afrique) et dans celui d'une divergence au large (Dôme de Costa Rica). Téthys., *6,* 157–170.

Minas, M. 1976. Production primaire, méthode ^{14}C, *in* Groupe Mediprod. Résultats de la campagne CINECA-5-J. CHARCOT-CAPRICORNE 7403 (1er Mars au 20 Avril 1974). Publ. CNEXO, sér. Résultats des campagnes à la mer, 10: 1.2.2.

Mittelstaedt, E., R. D. Pillsbury and R. L. Smith. 1975. Flow patterns in the northwest African upwelling area. Results of the measurements along 21° 40′ N during February-April 1974. JOINT I. Deutsche Hydrographische Zeitschrift, *28,* 145–167.

Neveux, J. 1976. Fluorescence *in vivo* et chlorophylle *a, in,* Groupe Mediprod. Résultats de la campagne CINECA-5-J. CHARCOT-CAPRICORNE 7403 (1er Mars au 20 Avril 1974). Publ. CNEXO, sér. Résultats des campagnes à la mer, 10: 1.1.3.

Packard, T. T. 1979. Respiration and respiratory electron transport activity in plankton from the northwest African upwelling area. J. Mar. Res., *37,* 711–742.

Redfield, A. C. 1948. The exchange of oxygen across the sea surface. J. Mar. Res., *7,* 347–361.

Redfield, A. C., B. Ketchum and F. A. Richards. 1963. The influence of organisms on the composition of sea water, *in* The Sea, M. N. Hill, ed., *2,* Wiley Interscience, New York, 554 pp.

Rowe, G. T., C. H. Clifford and K. L. Smith. 1977. Nutrient regeneration in sediments off Cape Blanc, Spanish Sahara. Deep-Sea Res., *24,* 57–63.

Ryther, J. H., D. W. Menzel, E. M. Hulburt, C. J. Lorenzen and N. Corwin. 1971. The production and utilization of organic matter in the Peru coastal current. Invest. Pesquera., *35*, 43–59.

Simpson, J. J. and A. Zirino. 1980. Biological control of pH in the Peruvian coastal upwelling area. Deep-Sea Res., *27*, 733–744.

Slawyk, G. and J. J. MacIsaac. 1972. Comparison of two automated ammonium methods in a region of coastal upwelling. Deep-Sea Res., *19*, 521–524.

Smith, S. L. and T. E. Whitledge. 1977. The role of zooplankton in the regeneration of nitrogen in a coastal upwelling system off northwest Africa. Deep-Sea Res., *24*, 49–56.

Steemann-Nielsen, E. 1952. The use of radioactive carbon (C^{14}) for measuring organic production in the sea. J. Cons. Perm. Intern. Explor. Mer., *18*, 117–140.

Strickland, J. D. H. and T. R. Parsons. 1968. A practical handbook of seawater analysis. Bull. Fish. Res. Bd. Can., *167*, 1–310.

Weiss, R. F. 1970. The solubility of nitrogen, oxygen and argon in water and seawater. Deep-Sea Res., *17*, 721–735.

Williams, P. J., R. C. T. Raine and J. R. Bryan. 1979. Agreement between the ^{14}C and oxygen methods of measuring phytoplankton production: reassessment of the photosynthetic quotient. Oceanol. Acta, *2*, 411–416.

Received: *20 August, 1981;* revised: *2 April, 1982.*